Tau misfolding efficiently propagates between individual intact hippocampal neurons

Abbreviated title: Efficient tau propagation between live neurons

Authors

Grace I Hallinan[1,3], Mariana Vargas-Caballero[1], Jonathan West[2], Katrin Deinhardt[1,4]

Affiliations

[1]Biological Sciences, University of Southampton, Southampton SO17 1BJ, UK

[2] Faculty of Medicine and Centre for Hybrid Biodevices, Institute for Life Sciences, University of Southampton, Southampton SO17 1BJ, UK

[3] Present address: Department of Pathology and Laboratory Medicine, Indiana University School of Medicine, Indianapolis, IN 46202, USA.

[4]Corresponding author. Contact: K.Deinhardt@soton.ac.uk

Number of pages: 30

Number of figures: 6

Number of words in abstract: 142; introduction: 645; discussion: 1226

Conflict of interests: The authors declare no competing financial interests.

Acknowledgements: This work was supported by Alzheimer's Research UK (grant numbers ARUK-PhD2014-10 and ARUK-PPG2017B-001) and the BBSRC (BB/L007576/1). We thank Professor Vincent O'Connor, Dr Amrit Mudher and Aleksandra Pitera for critically reading the manuscript.

Abstract

Neurofibrillary tangles, formed of misfolded, hyperphosphorylated tau protein, are a pathological hallmark of several neurodegenerations, including Alzheimer's disease. Tau pathology spreads between neurons and propagates misfolding in a prion-like manner throughout connected neuronal circuits. Tauopathy is accompanied by significant neuronal death, but the relationships between initial tau misfolding, propagation across connected neurons and cytotoxicity remain unclear. In particular the immediate functional consequence of tau misfolding for the individual neuron is not well understood. Here, using microfluidic devices to recreate discretely organised neuronal connections, we show that the spread and propagation of misfolded tau between individual murine neurons is rapid and efficient; it occurs within days. The neurons containing and propagating tau pathology display selective axonal transport deficits but remain viable and electrically competent. Therefore, we demonstrate that seed-competent misfolded tau species do not acutely cause cell death, but instead initiate discrete cellular dysfunctions.

Significance statement

Public awareness of progressive neurodegenerations such as dementias associated with ageing or repetitive head trauma is rising. Protein misfolding underlies many neurodegenerative diseases including tauopathies, where the misfolded tau protein propagates pathology through connected brain circuits in a prion-like manner. Clinically, these diseases progress over the course of years. Here we show that the underlying protein misfolding propagates rapidly between individual neurons. Presence of misfolded tau is not directly cytotoxic to the neuron; the cells remain viable with limited deficits. This suggests that neurons with tau pathology could be rescued with a therapeutic disease modifier and highlights an under-appreciated time window for such therapeutic intervention.

Introduction

Neurofibrillary tangles (NFTs), a pathological hallmark of several neurodegenerations including Alzheimer's disease (AD), consist of structured insoluble aggregates of hyperphosphorylated tau (Grundke-Iqbal et al., 1986). The neuroanatomical localisation of NFTs in AD brains suggests that tau pathology propagates through the brain along anterograde connected circuits (de Calignon et al., 2012; Ahmed et al., 2014). Indeed, it is well established that pathogenic tau spreads between cells *in vitro* (Frost et al., 2009; Sanders et al., 2014) and *in vivo* (de Calignon et al., 2012; Lasagna-Reeves et al., 2012; Liu et al., 2012) in a prion-like manner (Clavaguera et al., 2009; Frost et al., 2009; Kfoury et al., 2012; Kaufman et al., 2016). Tau oligomers of hyperphosphorylated tau have been isolated from patient brains (Köpke et al., 1993) and cause hyperphosphorylation and misfolding of native tau (Alonso et al., 1996; Li et al., 2007). The tau seeds that template the misfolded conformation to native tau are monomers or lower molecular weight oligomers (Michel et al., 2014; Falcon et al., 2015; Kim et al., 2015; Mirbaha et al., 2015; Jackson et al., 2016; Sharma et al., 2018), and as tau polymerises into filaments it loses seeding activity (Alonso et al., 2006).

Pathogenic tau causes cell death both *in vivo* (de Calignon et al., 2012) and *in vitro* (Gómez-Ramos et al., 2006; Tian et al., 2013), and advancement of AD is associated with extensive neuronal loss (Braak and Braak, 1991). Exogenous addition of tau is toxic to neurons *in vitro* (Gómez-Ramos et al., 2006; Kopeikina et al., 2012; Tian et al., 2013), suggesting that tau misfolding and aggregation is associated with neuronal death. Therefore, it has been suggested that tau seeds are released following the disintegration of the tangle-bearing neurons (Guo and Lee, 2011; Hu et al., 2016). This is consistent with *in vivo* observations where loss of neurons is progressive within brain areas affected by degeneration.

Interestingly, recent studies have detected tau species capable of seeding misfolding in

human brain areas free of tangle pathology (DeVos et al., 2018), implying that tau seed release occurs from intact neurons and precedes neuronal death (Pickett et al., 2017). By their nature these *in vivo* studies are short of the resolution required to identify the individual neurons bearing and releasing misfolded tau species, and as a consequence the physiological state of these neurons remains unclear.

To propagate pathology in a prion-like manner tau seeds spread to connected neurons and interact with native tau in the cytosol to template its misfolding. Studies using exogenous tau preparations to investigate the mechanisms underlying tau pathology transmission have shown that aggregates are internalised into primary neurons, trafficked both anterogradely and retrogradely along axons, spread to connected cells (Wu et al., 2013b, 2016; Takeda et al., 2015; Wang et al., 2017) and propagate tau pathology (Calafate et al., 2015; Wu et al., 2016; Nobuhara et al., 2017). However, the efficiency of propagation of tau misfolding between individual neurons and the consequence for the individual neuron's physiology have not been resolved.

In this study, we created a minimalistic neuronal circuit within a compartmentalised microfluidic device to investigate tau misfolding and propagation with single cell resolution. We show that a phosphomimetic tau, tau^{E14}, in which 14 disease-relevant serine/threonine residues have been mutated to glutamate to mimic phosphorylation (Hoover et al., 2010), misfolds within primary neurons in the absence of exogenous seeds. Misfolded tau^{E14} seeds template a rapid and efficient prion-like misfolding of native tau and transmit the conformational change of tau between intact, connected neurons with high efficiency. This suggests that propagation of misfolded tau occurs between live, functioning neurons in very early stages prior to neuronal degeneration. Our findings imply that propagation of misfolded tau through the brain likely precedes detectable symptoms, strengthening the idea that

targeting the spread of misfolded tau in as yet unaffected areas may present a disease modifying approach for mild cognitive impairment.

Materials and methods

Plasmids

The following plasmids were used: pRFP-N1, pEGFP-C3 (Clontech), pRK5-EGFP-tau^{WT} and pRK5-EGFP-tau^{E14} were a gift from Karen Ashe (Hoover et al., 2010) (Addgene plasmids #46904 and #46907), GCaMP6 was a gift from Douglas Kim (Chen et al., 2013) (Addgene plasmid #40753), R-GECO was a gift from Robert Campbell (Wu et al., 2013a) (Addgene plasmid #45494). RFP-tau^{WT} and RFP-tau^{E14} were created by excising the GFP fragment of pRK5-EGFP-Tau^{WT} at Cla1 and BamH1 sites, and replacing it with RFP, which was amplified by PCR with forward primer 5'-CATGATCGATATGGCCTCCTCC-3' and reverse primer 5'-CATGGGATCCGGCGCCGGT-3'.

Cell culture and transfection

All experiments were carried out in accordance with the Animals (Scientific Procedures) Act 1986 set out by the UK Home Office. Primary cultures were prepared as described previously (Deinhardt et al., 2011) from embryonic day 15-18 C57BL/6 mouse hippocampus. Dissociated neurons were plated in Neurobasal medium supplemented with 2% B27 and 0.5 mM GlutaMAX (Gibco) at a density of 7000 cells/µl in microfluidic devices, and 150,000 cells/ml in glass bottom dishes. Partial medium changes were performed on the devices every 2-3 days. On DIV1, neurons were transfected using Lipofectamine 2000 as described previously (Deinhardt et al., 2011). Transfection mix was added to device channels sequentially, and channels were fluidically isolated from each other through a volume difference to ensure no diffusion of the solution across channels (Dinh et al., 2013).

Microfluidic devices

Custom microfluidic devices were manufactured based on existing designs (Taylor et al., 2003; Peyrin et al., 2011). Devices were replicated as described (Holloway et al., 2019), washed in 70% EtOH for one hour and dried before use. Devices were mounted onto 22x55 mm coverslips (Smith Scientific) pretreated with 0.1 mg/ml poly-*D*-lysine (Sigma). Device channels were filled with supplemented Neurobasal medium and incubated overnight before addition of cells.

Immunocytochemistry

Neurons were fixed in 4% paraformaldehyde in PBS for 10–15 minutes, washed with 50 mM ammonium chloride in TBS for 5 minutes, and permeabilised in 0.1% Triton-X100 in TBS for 5 minutes at room temperature (RT). The cells were then blocked for 30 minutes in 10% goat serum in TBS at RT. Cells were incubated for 1 hour at RT or overnight at 4°C in the following primary antibodies: MC1 (1:300, gift from Peter Davies (Jicha et al., 1997)), synapsin-1 (D12G5, 1:1000, Cell Signalling). Primary antibody was washed off in TBS, and Hoechst (33342) was added to the second wash to stain nuclei (1:3000, Thermo Fisher). This was followed by incubation for 30 minutes at RT with fluorescently-conjugated secondary antibodies (Invitrogen).

Microscopy

Fixed cell images for axonal length analysis were taken on a Zeiss Axioplan Fluorescence Microscope equipped with a HBO103 Mercury lamp for illumination, a Qimaging Retiga 3000 monochrome CCD camera (Photometrics, UK), 20x/0.4NA and 40x/0.75NA Plan-Neofluar objectives, using Micro-manager software (Vale lab, USA). Fluorescent and differential interference contrast (DIC) images of cells in devices were obtained using a 60x/1.42NA Oil Plan APO objective on a DeltaVision Elite system (GE Life Sciences) with SSI 7-band LED for illumination and a monochrome sCMOS camera, using SoftWoRks software (version 6). Confocal images were taken on a Leica SP8 laser scanning confocal

149 microscope using a 63x/1.30NA HC Pl Apo CS2 glycerol immersion objective, with a PCO
150 Edge 5.5 sCMOS camera. Lasers used for illumination were continuous wave solid state
151 lasers at 405 and 561 nm, and a continuous wave argon gas laser at 488 nm.
152 Live cell imaging was performed on the DeltaVision Elite system (GE Life Sciences). For
153 imaging of lysosomes, DIV14 neurons were incubated with 25 nM LysoTracker Deep Red
154 (Thermo Fisher) for 20 minutes at 37°C. LysoTracker solution was then removed and
155 replaced with supplemented NBM containing 50 mM HEPES-NaOH, pH 7.4. Images were
156 taken at 0.2 Hz for 5 minutes. For calcium imaging, neurons were cotransfected with
157 GCaMP6 and RFP-Tau^{E14} or RFP-Tau^{WT}, or R-GECO and GFP-Tau^{E14} or GFP-Tau^{WT} and
158 imaged at DIV14 at 2 Hz for 6 minutes. After 3 min, 1 µM tetrodotoxin (Sigma) was added,
159 followed after 2 minutes by 100 mM KCl.
160 **Image analysis**
161 Overview images were reconstructed from multiple single images using Autostitch software
162 (University of British Columbia). Images were analysed using ImageJ software (NIH), and its
163 plugins NeuronJ (Meijering et al., 2004) and Iterative Deconvolution (Bob Dougherty).
164 Axonal length was defined as the longest axonal branch from the longest neurite. Distal axon
165 was defined as a 75 µm stretch of axon at, or near to, the terminal of an axon branch, and
166 proximal axon was defined as a 75 µm long stretch of axon measured beyond the first 50 µm
167 of axon protruding from the cell body, therefore beyond the axonal initial segment. Intensity
168 profiles along a line were generated using plot profile, and kymographs using the
169 MultipleKymograph plugin on ImageJ. Lysosomes which displaced greater than 50 µm over
170 the course of the time lapse were considered moving. Aggregate analysis was performed
171 using Matlab.
172 **Aggregate analysis**

The fluorescence intensity values of control and experimental axons were measured. Plot profiles of 75 µm long axonal stretches were generated from 16-bit images, and the pixel intensity values were analysed. To assess normal fluorescence fluctuations, a selection of intensity values derived from 50 control tau^{WT} axons across the time course were randomly chosen, and each was zeroed to its 10^{th} percentile. The mean+5 standard deviations of these values was calculated as 500 arbitrary units (a.u.). Therefore, tau^{WT} control axons with values above 500 a.u. were excluded from generating experimental control means, but included in the final analysis.

The fluorescence values for at least 12 control tau^{WT} and experimental tau^{E14} 75 µm long axonal stretches were analysed per timepoint, with three separate experiments per time point. The mean of the standard deviations of the control axons not excluded by the 500 a.u. cut-off was calculated. Any individual fluorescence value of tau^{WT} or tau^{E14} axons lying 5 times outside this mean was identified to be an aggregate-containing point. The sum of the aggregate-containing points was calculated for control tau^{WT} and experimental tau^{E14} axonal stretches, and from this the percentage of aggregate-containing values along an axonal stretch was calculated. Any axonal stretch that contains over 10% of its fluorescence values, i.e. over cumulative 7.5 µm of the analysed length, as aggregate-containing values was identified as axon positive for tau aggregation. This cut-off allows for intensity variations due to e.g. crossing axons to be discounted. Finally, the percentage of cells positive for tau aggregation is calculated for tau^{WT} and tau^{E14} expressing neurons.

Electrophysiology

Cells were cultured on coverslips and transfected with RFP-Tau^{WT} or RFP-Tau^{E14}. For patch clamp recording cells were perfused with oxygenated (95% O_2, 5% CO_2) artificial cerebrospinal fluid (CSF) which contained (in mM): 126 NaCl, 3 KCl, 1.25 NaH_2PO_4, 2 $MgSO_4$, 2 $CaCl_2$, 26 $NaHCO_3$, and 10 glucose, pH 7.3–7.4. at a rate of 1–2 ml/min.

Recordings were performed under visual control. Patch pipettes (4–6 MΩ) were pulled from thick-walled borosilicate glass tubing and filled with a solution containing (in mM): 110 K-Gluconate, 10 KCl, 10 Na-Phosphocreatine, 10 HEPES, 4 ATP-Mg, 0.3 GTP, (pH 7.25 adjusted with KOH; osmolarity 280 mosmol/l). Recordings were carried out at room temperature using an amplifier Axopatch 200B. After measurement of intrinsic membrane potential, if necessary, current was injected to maintain the membrane potential -75 ± 5 mV. All membrane potentials recorded were corrected off-line for liquid junction potential of -10 mV measured directly. Current pulses of increasing amplitude were used to test excitability in current clamp. Input resistance was measured in voltage clamp with 2 mV pulses. Signals were low-pass filtered at 5 kHz and sampled at 20 kHz with 16-bit resolution, using a National Instruments analogue card, and custom software written in Matlab and C (MatDAQ, Hugh Robinson, 1995–2013). All analysis was performed in Matlab.

Experimental Design and Statistical Analysis

All experiments contain data from a minimum of 3 independent dissections, with an individual experiment defined as the cells derived from embryos of one mouse. Statistical analysis was performed using GraphPad Prism 6 (Ver 6.00m Graph Pad Software Inc.). All data in text are expressed as mean ± SD, graphs show mean ± SEM. Statistical analyses were performed using a two-tailed t-test for comparison of two groups unless indicated otherwise, or an ANOVA for comparison of 3 or more groups, with details provided in the figure legends.

Results

Phosphomimetic tau spontaneously misfolds in cultured neurons.

Hyperphosphorylation of tau is associated with aggregation and pathology, and phosphomimetic tau (tau^{E14}) mislocalises to dendritic spines and causes synaptic dysfunction

(Hoover et al., 2010). To examine whether tau^{E14} spontaneously misfolds and forms visible aggregates, we cultured murine hippocampal neurons and transfected them at day *in vitro* (DIV) 1 with fluorescently tagged human 0N4R tau: GFP-tau^{E14} or RFP-tau^{E14} and GFP-tau^{WT} or RFP-tau^{WT}, respectively. Expression of either tau^{WT} or tau^{E14} did not adversely affect axonal outgrowth when compared to control neurons (Fig. 1a), and both wildtype (not shown) and mutant tau localised to intracellular structures (Fig. 1b). At DIV14, tau^{WT} displayed a smooth and even distribution throughout the cell, including along the axon. In contrast, tau^{E14} expression resulted in a clustered tau distribution, particularly along distal axons (Fig. 1c, d). Using an antibody that selectively recognises misfolded tau, MC1 (Jicha et al., 1997), we confirmed that the clustering of fluorescence reported tau misfolding within the cell. No misfolded tau was detected in axons exogenously expressing tau^{WT} (Fig. 1d), confirming that it is not a consequence of the introduction of human tau *per se*. This suggests that the fluorescence accumulations in the mutant tau expressing neurons represent either amorphous or structured build-ups of misfolded tau that we refer to as aggregates. In order to analyse the appearance of tau aggregation we generated fluorescence distribution profiles along individual axons. This confirmed highly variable fluorescence intensities along axons of tau^{E14} expressing neurons, in comparison to a smooth fluorescence distribution in tau^{WT} expressing neurons (Fig.1c). At DIV14, 56.0 ± 7.7% of the tau^{E14} expressing axons have developed aggregates, whereas the distal axons of tau^{WT} expressing neurons remained aggregate-free. This demonstrates that tau phosphorylation is sufficient to induce its misfolding and aggregation.

Tau misfolding efficiently propagates to connected neurons.

Untransfected neurites in the vicinity of a tau^{E14} expressing axon were positive for misfolded tau (Fig. 1d, arrows). This suggests that tau^{E14} expression is sufficient not only to induce

misfolding and aggregation of tau within the axon, but also to generate seeds that spread to neighbouring cells. To more precisely investigate the spread and propagation of tau misfolding and aggregation between neurons, we co-cultured tau^{E14} expressing 'donor' cells and tau^{WT} 'acceptor' cells within a microfluidic device that allows co-culture of two spatially distinct neuronal populations that can be manipulated independently but are in contact via projecting axons (Taylor et al., 2005; Wu et al., 2013b). This enabled us to separate tau^{E14} and tau^{WT} expressing neurons and identify individual connecting cells (Fig. 2a-c). Aggregates were first detected at DIV8 in the axons of tau^{E14} expressing donor neurons (Fig. 2e), and the number of axons positive for tau aggregation steadily increased at a rate of 4.9 ± 0.6% per day, until a plateau was reached at DIV18 with 75.5 ± 6.4% of axons containing visible tau aggregates (Fig. 2e). Next, we analysed the percentage of aggregate positive acceptor neurons to assess if propagation occurs in our system. We first detected aggregates in tau^{WT} acceptor axons connected to tau^{E14} expressing donor neurons at DIV10, and their percentage increased over time by 4.9 ± 0.4% additional distal acceptor axons positive for tau aggregation per day (Fig. 2d, e). They thus followed the donor neurons with a delay of ~3.7 days, until 77.5 ± 7.8% of distal axons contained tau aggregates, reaching the same plateau as donor distal axons ($p>0.999$ between donor and acceptor axons at DIV24 and DIV26) (Fig. 2e). No aggregation was detected when tau^{WT} acceptor neurons were connected to GFP or GFP-tau^{WT} expressing control cells, demonstrating a clear difference in conformation of tau^{WT} dependent on the type of donor cell to which it connects ($p<0.0001$) (Fig. 2d, e). This demonstrates that within a minimal neuronal circuit, expression of phosphomimetic tau in primary hippocampal neurons prompts tau misfolding and the generation of tau seeds, which rapidly and efficiently transfer to connected cells where they propagate aggregation of tau in a prion-like manner.

Distinct neuronal subcompartments display a differential vulnerability to tau misfolding and aggregation.

In both the donor (not shown) and acceptor neurons, tau aggregates first appeared in the distal axon, and were later detected in the somatodendritic compartment (Fig. 3a). For distal axonal misfolding and aggregation to occur in the acceptor neuron within the oriented setup of the microfluidic chamber (Fig. 2a, b), seeds that have been internalised at the somatodendritic compartment must have been transported to the distal axon, or alternatively, must have propagated the conformational change throughout the cell. Indeed, we detected GFP-tau^{E14} positive accumulations in the somata of RFP-tau^{WT} expressing neurons (Fig. 3b), indicating transfer of tau^{E14} to the connected neuron. No aggregates were visible within the somata of tau^{WT} expressing neurons connected to GFP expressing cells (Fig. 3c). The aggregates within the tau^{WT} expressing somata were dual positive for GFP-tau^{E14} and RFP-tau^{WT}, demonstrating that the phosphomimetic tau had further recruited native tau into aggregates (Fig. 3b), thus suggesting a prion-like propagation of aggregation. We confirmed that the misfolding of tau was propagated to the distal axons of acceptor cells using MC1 staining (Fig. 3d). No GFP-tau^{E14} was detected in the tau accumulations of RFP-tau^{WT} expressing axons (not shown), substantiating that tau^{E14} seeded the misfolding of tau^{WT}. This demonstrates that as well as being sufficient for inducing tau aggregate formation, mimicking phosphorylation of tau is sufficient for the prion-like propagation of the conformational change to surrounding neurons. Interestingly, we never detected tau aggregation at the proximal axonal segment of either donor or acceptor neurons, and this axonal subcompartment also remained negative for MC1 staining indicating absence of misfolded species (Fig. 3d). Together with the observation that visible tau aggregates were first observed in the distal axon of acceptor cells, despite receiving the seeds at the somatodendritic compartment, this suggests that (i) smaller seeds distribute throughout the

297 neuron prior to the formation of visible aggregates, (ii) tau in the distal axon is most
298 susceptible to aggregation and (iii) misfolded tau does not accumulate in, or is rapidly cleared
299 from, the proximal axonal region.
300
301 **Misfolded tau is not acutely toxic.**
302 We monitored the formation and propagation of tau pathology at the single cell level, and
303 thus were able to analyse the state of tau^{E14} expressing cells at the time of misfolding and
304 active tau seed transmission and propagation of misfolding. Loss of synaptic connections has
305 been identified as one of the earliest cellular changes in Alzheimer's disease (Scheff et al.,
306 1990; Masliah et al., 2001). As tau misfolding and aggregation first occur in the distal axon
307 we visualised a presynaptic marker, synapsin, to assess the density of presynaptic sites in
308 tau^{E14} expressing donor neurons at a time point of active tau seed propagation (DIV14).
309 There was no significant difference in the number of presynaptic sites between tau^{WT} and
310 tau^{E14} expressing neurons and their untransfected surrounding axons ($p=0.82$, Fig. 4a-c). In
311 fact, the neurons appear intact and undistinguishable from surrounding untransfected cells, as
312 judged by differential interference contrast (DIC) imaging, exhibiting a smooth and intact
313 plasma membrane and healthy nuclear morphology (Fig. 4a). This suggests that the presence
314 and release of misfolded tau seeds are not acutely toxic to hippocampal neurons. Indeed, we
315 did not observe disintegration or death of these neurons across the analysed time course to
316 DIV26 and beyond.
317 We next investigated the physiological state of aggregate-containing neurons in more detail
318 to assess the functional consequences. Because tau acts in microtubule stabilisation (Drubin
319 and Kirschner, 1986), and its dysfunction leads to axonal transport deficits (Alonso et al.,
320 1994; Mandelkow et al., 2003), we first assessed lysosome dynamics. Lysosomes are
321 transported bi-directionally along axons (Che et al., 2016). At DIV14 there was a significant

decrease in the number of lysosomes present at the distal axon of tau^{E14} expressing neurons compared to tau^{WT} controls (p=0.0017, Fig. 5a, b). Of those lysosomes present, a significantly lower percentage were moving within tau^{E14} axons (21.1 ± 3.9%) compared to tau^{WT} controls (45.8 ± 5.8%, p=0.0036) (Fig. 5c-e), confirming an early axonal transport dysfunction in the presence of tau misfolding.

To confirm our observation that neurons expressing tau^{E14} remained viable in the presence of misfolded tau we then visualised spontaneous activity using calcium imaging (Fig. 6a, b). Both tau^{WT} and tau^{E14} expressing neurons displayed calcium fluxes that were sensitive to tetrodotoxin, showing that they were driven by voltage-gated sodium channels. This demonstrates that energy-dependent processes were functional and suggests that neurons remain electrically competent in the presence of misfolded and aggregated tau. To investigate the electrical competence in more detail we performed electrophysiological analysis on the cells with whole-cell patch clamp. Both tau^{E14} and tau^{WT} expressing neurons were capable of responding to positive current injections with action potentials of a similar amplitude (Fig. 6c). There were no significant differences in the minimum current required to evoke a single action potential (rheobase); with tau^{E14} and tau^{WT} expressing neurons requiring 77 ± 40 pA and 83 ± 25 pA respectively (p = 0.82) (Fig. 6d). We further found no significant differences in the input resistance between tau^{E14} (694 ± 367 MΩ) and tau^{WT} (578 ± 101 MΩ) expressing cells, (p = 0.62) (Fig. 6e), and the resting membrane potentials of tau^{E14} (-73.8 ± 2.4 mV) and tau^{WT} (-73.3 ± 3.5 mV) expressing neurons did not differ (p = 0.85) (Fig. 6f). This shows that despite possessing and transmitting tau pathology, donor neurons maintain a normal resting membrane potential and fire action potentials to the same extent as tau^{WT} control neurons. Together, these data demonstrate that phosphomimetic tau misfolds and aggregates in the absence of exogenous seeds, and that transmission of tau misfolding to healthy neurons is an active and efficient process that is accompanied by selective neuronal dysfunction. The

presence of misfolded and aggregated tau does not compromise neuronal excitability and is compatible with longer-term neuronal viability.

Discussion

What triggers the initial tau seed formation *in vivo* is unclear, and there is currently a debate as to the nature of this propagative species (Michel et al., 2014; Mirbaha et al., 2015; Sharma et al., 2018). The presence of mutations increases the propensity of seed formation (Gao et al., 2018), and tau aggregation is associated with hyperphoshorylation (Alonso et al., 1996; Wang et al., 1996, 2007). Indeed, AD is associated with an imbalance of kinase and phosphatase activities (Stoothoff and Johnson, 2005) that leads to hyperphosphorylation of tau, detectable within NFTs (Hanger et al., 2009). We here show that the negative charges conferred by a phosphomimetic tau, which simulates hyperphosphorylation at 14 disease-related sites, do not interfere with localisation to subcellular structures, but are sufficient to initiate tau misfolding and aggregation within a living neuron in the absence of exogenous seeds. Previous work showed that when using recombinant seeds, the efficiency of seeding is decreased in the presence of hyperphosphorylation (Falcon et al., 2015), and tau seeds isolated from tgP301S tau mouse brains more potently seed misfolding than tau seeds formed *in vitro*. This increased potency of tgP301S seeds is retained upon amplification with recombinantly generated tau protein that is not post-translationally modified (Falcon et al., 2015). Together with our data this suggests that hyperphosphorylation itself does not interfere with subcellular tau localisation nor dictate misfolding. However, within a cellular environment the negative charges associated with hyperphosphorylation increase the propensity for folding into an alternative structure that can act as an efficient seed for native tau to misfold, aggregate and propagate.

The compartmented setup of the device propagation assay allowed us to monitor individual neurons that formed or received misfolded tau species. This allowed for the first time, an analysis of propagation efficiency, and showed unexpectedly fast and robust tau propagation from neuron to neuron *in vitro* with a near complete transmission efficiency. Our study used pure murine hippocampal neurons, cultured in the absence of other cell types. The high efficiency of transmission may be due to a lack of a glial population, which display tau pathology in patients with tauopathy (Arai et al., 2001; Spillantini et al., 1997, 1998), as well as in *in vivo* (Clavaguera et al., 2013) and *in vitro* (Bolós et al., 2015) models of tauopathy. Therefore, glial populations may play a role in clearance of secreted pathogenic tau, and their absence in our setup revealed an under-appreciated intrinsic high efficiency of tau release and re-uptake in neurons. Synaptic contacts have been shown to enhance tau propagation *in vitro* (Calafate et al., 2015; Wang et al., 2017), however our system shows tau propagation at earlier time points than mature synapse formation (Ichikawa et al., 1993), and no increased rate of propagation after this time point. This high efficiency of neuron-to-neuron tau propagation suggests that a physiological process of protein transmission may be at play that is occurring in healthy neurons but is only revealed under pathological conditions through transmission of a conformationally altered species. This idea is reinforced by the observation that healthy tau is secreted from intact neurons in an activity-dependent manner (Pooler et al., 2013). The rapid and efficient propagation of tau misfolding in our system is at odds with findings that show Braak staging progresses in patients over a matter of years to decades (Braak et al., 2011). This staging measures the presence of NFTs, which are highly structured end-stage tau assemblies within dead or dying neuronal cells. The discrepancy may thus result from the fact that we measured early events of tau misfolding in response to exogenously expressed mutant tau. The timing with which initial misfolding of tau converts to cellular degeneration, tangle formation and cytotoxicity remains unclear. The connected

compartmentalised setup used in this study allows direct investigation of individual neurons that initiate and propagate misfolding, or that receive transmitted tau seeds, at single cell and subcellular level. This revealed compartmentalised tau aggregation within individual neurons that begins within the distal axon, regardless of whether misfolding was originally initiated within the cell or transmitted to it. This spatial organisation holds true despite the oriented setup of connected neurons, where tau seeds first enter the receiving neurons at the somatodendritic region; the site furthest from the distal axon where aggregation is initiated. Only later were aggregates visible within the somata. This confirms that the *in vitro* setup faithfully replicates *in vivo* observations describing pathological tau present in axonal tracts prior to its appearance in the somatodendritic compartment (Christensen et al., 2019), and prior to the neuropil threads seen in advanced AD (Braak et al., 1986). Furthermore, we did not observe tau aggregates in the proximal axonal segment, even at stages where clear aggregates were visible in both the soma and distal axon. This suggests either a selective vulnerability of the distal axonal segment, or protection against tau misfolding in proximal axonal regions. The axon initial segment has been shown to act as a barrier for select isoforms of tau proteins, potentially due to increased microtubule dynamics in this area (Sohn et al., 2016; Zempel et al., 2017), which may play a role in the lack of retention of misfolded tau within this region. However, it is clear from our data that misfolded tau is able to cross this barrier and cause distal axon pathology.

In vivo paradigms do not yet facilitate the direct visualisation of neurons that are actively releasing and propagating tau pathology. Monitoring tau misfolding and aggregation within single cells allowed us to directly assess the physiological effects that tau misfolding has on neurons. We found that despite containing and propagating misfolded tau for prolonged periods of time, neurons remained alive, functional, and retained energy dependent processes, yet displayed a selective dysfunction in axonal transport. Previous studies showed that

acutely added tau seeds can induce toxicity and cell death via calcium dysregulation (Gómez-Ramos et al., 2006; Kopeikina et al., 2012; Tian et al., 2013). However, we found that neurons containing self-generated tau aggregates had intact calcium fluxes, physiological resting membrane potentials, were able to elicit action potentials and remained viable for extended periods of time after initial tau misfolding, aggregate formation and propagation. Our data therefore shows that misfolded tau and tau aggregates are not themselves lethal to neurons. Instead, they initiate a selective axonal transport dysfunction that precedes synaptic loss, and in isolation does not result in axonal degeneration or cell death. Furthermore, this compartmentalised assay provides the first direct evidence showing that tau pathology propagation can occur between live and functioning cells and precedes synaptic or neuronal degeneration. Interestingly, prion seeds are detected throughout all brain regions in mice infected with prion disease, while degeneration is region specific (Alibhai et al., 2016). Together, these data and our findings suggest that the idea that the presence of misfolded protein in isolation does not determine neurodegeneration (Alibhai et al., 2016) may hold true across different protein misfolding diseases. Combined with a potential physiological transmission of tau between neurons, this raises the possibility that at the stage of diagnosis, tau seeds may have spread throughout wider brain regions, having passed the time point where a sequestration of free tau seeds in isolation is effective in halting disease progression. However, our data imply that because the affected neurons are intact and viable at the early stages of tau misfolding, neurons containing early tau pathology could potentially be rescued.

441 **References**

442 Ahmed Z, Cooper J, Murray TK, Garn K, McNaughton E, Clarke H, Parhizkar S, Ward MA,
443 Cavallini A, Jackson S, Bose S, Clavaguera F, Tolnay M, Lavenir I, Goedert M, Hutton
444 ML, O'Neill MJ (2014) A novel in vivo model of tau propagation with rapid and
445 progressive neurofibrillary tangle pathology: the pattern of spread is determined by
446 connectivity, not proximity. Acta Neuropathol 127:667–683.

447 Alibhai J, Blanco RA, Barria MA, Piccardo P, Caughey B, Perry VH, Freeman TC, Manson
448 JC (2016) Distribution of Misfolded Prion Protein Seeding Activity Alone Does Not
449 Predict Regions of Neurodegeneration Bates GP, ed. PLOS Biol 14:e1002579.

450 Alonso A d. C, Li B, Grundke-Iqbal I, Iqbal K (2006) Polymerization of
451 hyperphosphorylated tau into filaments eliminates its inhibitory activity. Proc Natl Acad
452 Sci 103:8864–8869.

453 Alonso AC, Grundke-Iqbal I, Iqbal K (1996) Alzheimer's disease hyperphosphorylated tau
454 sequesters normal tau into tangles of filaments and disassembles microtubules. Nat Med
455 2:783–787.

456 Alonso AC, Zaidi T, Grundke-Iqbal I, Iqbal K (1994) Role of abnormally phosphorylated tau
457 in the breakdown of microtubules in Alzheimer disease. Proc Natl Acad Sci U S A
458 91:5562–5566.

459 Arai T A, Ikeda K, Akiyama H, Shikamoto Y, Tsuchiya K, Yagishita S, Beach T, Rogers J,
460 Schwab C, McGeer PL (2001) Distinct isoforms of tau aggregated in neurons and glial
461 cells in brains of patients with Pick's disease, corticobasal degeneration and progressive
462 supranuclear palsy. Acta Neuropathol 101:167–173.

463 Bolós M, Llorens-Martín M, Jurado-Arjona J, Hernández F, Rábano A, Avila J (2015) Direct
464 Evidence of Internalization of Tau by Microglia In Vitro and In Vivo. J Alzheimer's Dis
465 50:77–87.

466 Braak H, Braak E (1991) Neuropathological stageing of Alzheimer-related changes. Acta
467 Neuropathol 82:239–259.
468 Braak H, Braak E, Grundke-Iqbal I, Iqbal K (1986) Occurrence of neuropil threads in the
469 senile human brain and in Alzheimer's disease: A third location of paired helical
470 filaments outside of neurofibrillary tangles and neuritic plaques. Neurosci Lett 65:351–
471 355.
472 Braak H, Thal DR, Ghebremedhin E, Del Tredici K (2011) Stages of the Pathologic Process
473 in Alzheimer Disease: Age Categories From 1 to 100 Years. J Neuropathol Exp Neurol
474 70:960–969.
475 Calafate S, Buist A, Miskiewicz K, Vijayan V, Daneels G, de Strooper B, de Wit J,
476 Verstreken P, Moechars D (2015) Synaptic Contacts Enhance Cell-to-Cell Tau
477 Pathology Propagation. Cell Rep 11:1176–1183.
478 Che DL, Chowdary PD, Cui B (2016) A close look at axonal transport: Cargos slow down
479 when crossing stationary organelles. Neurosci Lett 610:110–116.
480 Chen T-W, Wardill TJ, Sun Y, Pulver SR, Renninger SL, Baohan A, Schreiter ER, Kerr RA,
481 Orger MB, Jayaraman V, Looger LL, Svoboda K, Kim DS (2013) Ultrasensitive
482 fluorescent proteins for imaging neuronal activity. Nature 499:295–300.
483 Christensen KR, Beach TG, Serrano GE, Kanaan NM (2019) Pathogenic tau modifications
484 occur in axons before the somatodendritic compartment in mossy fiber and Schaffer
485 collateral pathways. Acta Neuropathol Commun 7:29.
486 Clavaguera F, Akatsu H, Fraser G, Crowther RA, Frank S, Hench J, Probst A, Winkler DT,
487 Reichwald J, Staufenbiel M, Ghetti B, Goedert M, Tolnay M (2013) Brain homogenates
488 from human tauopathies induce tau inclusions in mouse brain. Proc Natl Acad Sci U S A
489 110:9535–9540.
490 Clavaguera F, Bolmont T, Crowther RA, Abramowski D, Frank S, Probst A, Fraser G,

Stalder AK, Beibel M, Staufenbiel M, Jucker M, Goedert M, Tolnay M (2009) Transmission and spreading of tauopathy in transgenic mouse brain. Nat Cell Biol 11:909–913.

de Calignon A, Polydoro M, Suárez-Calvet M, William C, Adamowicz DH, Kopeikina KJ, Pitstick R, Sahara N, Ashe KH, Carlson GA, Spires-Jones TL, Hyman BT (2012) Propagation of Tau Pathology in a Model of Early Alzheimer's Disease. Neuron 73:685–697.

Deinhardt K, Kim T, Spellman DS, Mains RE, Eipper BA, Neubert TA, Chao MV., Hempstead BL (2011) Neuronal growth cone retraction relies on proneurotrophin receptor signaling through Rac. Sci Signal 4:ra82.

DeVos SL, Corjuc BT, Oakley DH, Nobuhara CK, Bannon RN, Chase A, Commins C, Gonzalez JA, Dooley PM, Frosch MP, Hyman BT (2018) Synaptic Tau Seeding Precedes Tau Pathology in Human Alzheimer's Disease Brain. Front Neurosci 12:267.

Dinh N-D, Chiang Y-Y, Hardelauf H, Baumann J, Jackson E, Waide S, Sisnaiske J, Frimat J-P, van Thriel C, Janasek D, Peyrin J-M, West J (2013) Microfluidic construction of minimalistic neuronal co-cultures. Lab Chip 13:1402–1412.

Drubin DG, Kirschner MW (1986) Tau protein function in living cells. J Cell Biol 103:2739–2746.

Falcon B, Cavallini A, Angers R, Glover S, Murray TK, Barnham L, Jackson S, O'Neill MJ, Isaacs AM, Hutton ML, Szekeres PG, Goedert M, Bose S (2015) Conformation determines the seeding potencies of native and recombinant Tau aggregates. J Biol Chem 290:1049–1065.

Frost B, Jacks RL, Diamond MI (2009) Propagation of tau misfolding from the outside to the inside of a cell. J Biol Chem 284:12845–12852.

Gao Y-L, Wang N, Sun F-R, Cao X-P, Zhang W, Yu J-T (2018) Tau in neurodegenerative

disease. Ann Transl Med 6:175–175.

Gómez-Ramos A, Díaz-Hernández M, Cuadros R, Hernández F, Avila J (2006) Extracellular tau is toxic to neuronal cells. FEBS Lett 580:4842–4850.

Grundke-Iqbal I, Iqbal K, Tung YC, Quinlan M, Wisniewski HM, Binder LI (1986) Abnormal phosphorylation of the microtubule-associated protein tau (tau) in Alzheimer cytoskeletal pathology. Proc Natl Acad Sci 83:4913–4917.

Guo JL, Lee VM-Y (2011) Seeding of normal Tau by pathological Tau conformers drives pathogenesis of Alzheimer-like tangles. J Biol Chem 286:15317–15331.

Hanger DP, Anderton BH, Noble W (2009) Tau phosphorylation: the therapeutic challenge for neurodegenerative disease. Trends Mol Med 15:112–119.

Holloway PM, Hallinan GI, Hegde M, Lane SIR, Deinhardt K, West JJ (2019) Asymmetric confinement for defining outgrowth directionality. Lab Chip 19:1484–1489.

Hoover BR, Reed MN, Su J, Penrod RD, Kotilinek LA, Grant MK, Pitstick R, Carlson GA, Lanier LM, Yuan L-L, Ashe KH, Liao D (2010) Tau mislocalization to dendritic spines mediates synaptic dysfunction independently of neurodegeneration. Neuron 68:1067–1081.

Hu W, Zhang X, Tung YC, Xie S, Liu F, Iqbal K (2016) Hyperphosphorylation determines both the spread and the morphology of tau pathology. Alzheimer's Dement 12:1066–1077.

Ichikawa M, Muramoto K, Kobayashi K, Kawahara M, Kuroda Y (1993) Formation and maturation of synapses in primary cultures of rat cerebral cortical cells: an electron microscopic study. Neurosci Res 16:95–103.

Jackson SJ, Kerridge C, Cooper J, Cavallini A, Falcon B, Cella C V, Landi A, Szekeres PG, Murray TK, Ahmed Z, Goedert M, Hutton M, O'Neill MJ, Bose S (2016) Short Fibrils Constitute the Major Species of Seed-Competent Tau in the Brains of Mice Transgenic

for Human P301S Tau. J Neurosci 36:762–772.

Jicha GA, Bowser R, Kazam IG, Davies P (1997) Alz-50 and MC-1, a new monoclonal antibody raised to paired helical filaments, recognize conformational epitopes on recombinant tau. J Neurosci Res 48:128–132.

Kaufman SK, Sanders DW, Thomas TL, Ruchinskas AJ, Vaquer-Alicea J, Sharma AM, Miller TM, Diamond MI (2016) Tau Prion Strains Dictate Patterns of Cell Pathology, Progression Rate, and Regional Vulnerability In Vivo. Neuron 92:796–812.

Kfoury N, Holmes BB, Jiang H, Holtzman DM, Diamond MI (2012) Trans-cellular propagation of Tau aggregation by fibrillar species. J Biol Chem 287:19440–19451.

Kim D, Lim S, Haque MM, Ryoo N, Hong HS, Rhim H, Lee D-E, Chang Y-T, Lee J-S, Cheong E, Kim DJ, Kim YK (2015) Identification of disulfide cross-linked tau dimer responsible for tau propagation. Sci Rep 5:15231.

Kopeikina KJ, Hyman BT, Spires-Jones TL (2012) Soluble forms of tau are toxic in Alzheimer's disease. Transl Neurosci 3:223–233.

Köpke E, Tung YC, Shaikh S, Alonso AC, Iqbal K, Grundke-Iqbal I (1993) Microtubule-associated protein tau. Abnormal phosphorylation of a non-paired helical filament pool in Alzheimer disease. J Biol Chem 268:24374–24384.

Lasagna-Reeves CA, Castillo-Carranza DL, Sengupta U, Guerrero-Munoz MJ, Kiritoshi T, Neugebauer V, Jackson GR, Kayed R (2012) Alzheimer brain-derived tau oligomers propagate pathology from endogenous tau. Sci Rep 2:700.

Li B, Chohan MO, Grundke-Iqbal I, Iqbal K (2007) Disruption of microtubule network by Alzheimer abnormally hyperphosphorylated tau. Acta Neuropathol 113:501–511.

Liu L, Drouet V, Wu JW, Witter MP, Small SA, Clelland C, Duff K (2012) Trans-Synaptic Spread of Tau Pathology In Vivo Ikezu T, ed. PLoS One 7:e31302.

Mandelkow E-M, Stamer K, Vogel R, Thies E, Mandelkow E (2003) Clogging of axons by

566 tau, inhibition of axonal traffic and starvation of synapses. Neurobiol Aging 24:1079–
567 1085.
568 Masliah E, Mallory M, Alford M, DeTeresa R, Hansen LA, McKeel DW, Morris JC (2001)
569 Altered expression of synaptic proteins occurs early during progression of Alzheimer's
570 disease. Neurology 56:127–129.
571 Meijering E, Jacob M, Sarria J-CF, Steiner P, Hirling H, Unser M (2004) Design and
572 validation of a tool for neurite tracing and analysis in fluorescence microscopy images.
573 Cytometry 58A:167–176.
574 Michel CH, Kumar S, Pinotsi D, Tunnacliffe A, St George-Hyslop P, Mandelkow E,
575 Mandelkow E-M, Kaminski CF, Kaminski Schierle GS (2014) Extracellular monomeric
576 tau protein is sufficient to initiate the spread of tau protein pathology. J Biol Chem
577 289:956–967.
578 Mirbaha H, Holmes BB, Sanders DW, Bieschke J, Diamond MI (2015) Tau Trimers Are the
579 Minimal Propagation Unit Spontaneously Internalized to Seed Intracellular Aggregation.
580 J Biol Chem 290:14893–14903.
581 Nobuhara CK et al. (2017) Tau Antibody Targeting Pathological Species Blocks Neuronal
582 Uptake and Interneuron Propagation of Tau in Vitro. Am J Pathol 187:1399–1412.
583 Peyrin J-M, Deleglise B, Saias L, Vignes M, Gougis P, Magnifico S, Betuing S, Pietri M,
584 Caboche J, Vanhoutte P, Viovy J-L, Brugg B (2011) Axon diodes for the reconstruction
585 of oriented neuronal networks in microfluidic chambers. Lab Chip 11:3663–3673.
586 Pickett EK, Henstridge CM, Allison E, Pitstick R, Pooler A, Wegmann S, Carlson G, Hyman
587 BT, Spires-Jones TL (2017) Spread of tau down neural circuits precedes synapse and
588 neuronal loss in the rTgTauEC mouse model of early Alzheimer's disease. Synapse
589 71:e21965.
590 Pooler AM, Phillips EC, Lau DHW, Noble W, Hanger DP (2013) Physiological release of

591 endogenous tau is stimulated by neuronal activity. EMBO Rep 14:389–394.
592 Sanders DW, Kaufman SK, DeVos SL, Sharma AM, Mirbaha H, Li A, Barker SJ, Foley AC,
593 Thorpe JR, Serpell LC, Miller TM, Grinberg LT, Seeley WW, Diamond MI (2014)
594 Distinct tau prion strains propagate in cells and mice and define different tauopathies.
595 Neuron 82:1271–1288.
596 Scheff SW, DeKosky ST, Price DA (1990) Quantitative assessment of cortical synaptic
597 density in Alzheimer's disease. Neurobiol Aging 11:29–37.
598 Sharma AM, Thomas TL, Woodard DR, Kashmer OM, Diamond MI (2018) Tau monomer
599 encodes strains. Elife 7.
600 Sohn PD, Tracy TE, Son H-I, Zhou Y, Leite REP, Miller BL, Seeley WW, Grinberg LT, Gan
601 L (2016) Acetylated tau destabilizes the cytoskeleton in the axon initial segment and is
602 mislocalized to the somatodendritic compartment. Mol Neurodegener 11:47.
603 Spillantini MG, Crowther RA, Kamphorst W, Heutink P, van Swieten JC (1998) Tau
604 Pathology in Two Dutch Families with Mutations in the Microtubule-Binding Region of
605 Tau. Am J Pathol 153:1359–1363.
606 Spillantini MG, Goedert M, Crowther RA, Murrell JR, Farlow MR, Ghetti B (1997) Familial
607 multiple system tauopathy with presenile dementia: A disease with abundant neuronal
608 and glial tau filaments. Proc Natl Acad Sci 94.
609 Stoothoff WH, Johnson GVW (2005) Tau phosphorylation: physiological and pathological
610 consequences. Biochim Biophys Acta 1739:280–297.
611 Takeda S, Wegmann S, Cho H, DeVos SL, Commins C, Roe AD, Nicholls SB, Carlson GA,
612 Pitstick R, Nobuhara CK, Costantino I, Frosch MP, Müller DJ, Irimia D, Hyman BT
613 (2015) Neuronal uptake and propagation of a rare phosphorylated high-molecular-
614 weight tau derived from Alzheimer's disease brain. Nat Commun 6:8490.
615 Taylor AM, Blurton-Jones M, Rhee SW, Cribbs DH, Cotman CW, Jeon NL (2005) A

616 microfluidic culture platform for CNS axonal injury, regeneration and transport. Nat
617 Methods 2:599–605.
618 Taylor AM, Rhee SW, Tu CH, Cribbs DH, Cotman CW, Jeon NL (2003) Microfluidic
619 Multicompartment Device for Neuroscience Research. Langmuir 19:1551–1556.
620 Tian H, Davidowitz E, Lopez P, Emadi S, Moe J, Sierks M (2013) Trimeric tau is toxic to
621 human neuronal cells at low nanomolar concentrations. Int J Cell Biol 2013:260787.
622 Wang J-Z, Grundke-Iqbal I, Iqbal K (2007) Kinases and phosphatases and tau sites involved
623 in Alzheimer neurofibrillary degeneration. Eur J Neurosci 25:59–68.
624 Wang JZ, Grundke-Iqbal I, Iqbal K (1996) Restoration of biological activity of Alzheimer
625 abnormally phosphorylated tau by dephosphorylation with protein phosphatase-2A, -2B
626 and -1. Brain Res Mol Brain Res 38:200–208.
627 Wang Y, Balaji V, Kaniyappan S, Krüger L, Irsen S, Tepper K, Chandupatla R, Maetzler W,
628 Schneider A, Mandelkow E, Mandelkow E-M (2017) The release and trans-synaptic
629 transmission of Tau via exosomes. Mol Neurodegener 12:5.
630 Wu J, Liu L, Matsuda T, Zhao Y, Rebane A, Drobizhev M, Chang Y-F, Araki S, Arai Y,
631 March K, Hughes TE, Sagou K, Miyata T, Nagai T, Li W-H, Campbell RE (2013a)
632 Improved orange and red $Ca^{2}\pm$ indicators and photophysical considerations for
633 optogenetic applications. ACS Chem Neurosci 4:963–972.
634 Wu JW, Herman M, Liu L, Simoes S, Acker CM, Figueroa H, Steinberg JI, Margittai M,
635 Kayed R, Zurzolo C, Di Paolo G, Duff KE (2013b) Small misfolded Tau species are
636 internalized via bulk endocytosis and anterogradely and retrogradely transported in
637 neurons. J Biol Chem 288:1856–1870.
638 Wu JW, Hussaini SA, Bastille IM, Rodriguez GA, Mrejeru A, Rilett K, Sanders DW, Cook
639 C, Fu H, Boonen RACM, Herman M, Nahmani E, Emrani S, Figueroa YH, Diamond
640 MI, Clelland CL, Wray S, Duff KE (2016) Neuronal activity enhances tau propagation

641 and tau pathology in vivo. Nat Neurosci 19:1085–1092.
642 Zempel H, Dennissen FJA, Kumar Y, Luedtke J, Biernat J, Mandelkow E-M, Mandelkow E
643 (2017) Axodendritic sorting and pathological missorting of Tau are isoform-specific and
644 determined by axon initial segment architecture. J Biol Chem 292:12192–12207.
645

Figure legends

Figure 1. Tau aggregates spontaneously develop in GFP-tau^{E14} expressing hippocampal neurons. (a) Hippocampal neurons were transfected with GFP, GFP-tau^{WT} or GFP-tau^{E14} at DIV1 and fixed and imaged at DIV7. No difference in axonal outgrowth was observed. Each data point is one axon, n≥18 axons per condition from 3 experiments. One-way ANOVA, p=0.98, $F_{2,55}$ = 0.017. Error bars=SEM. (b) A higher magnification view of a hippocampal neuron transfected with GFP-tau^{E14} at DIV1 and fixed and imaged at DIV14. All scale bars, 10 µm. (c) A line was drawn along distal axons expressing tau^{WT} (top, magenta) or tau^{E14} (middle, green) to generate corresponding intensity profiles (bottom). Scale bar, 5 µm. (d) Tau^{E14} and surrounding untransfected axons (arrows), but not tau^{WT} expressing axons are positive for misfolded tau. Scale bar, 5 µm.

Figure 2. Tau misfolding efficiently propagates to connected neurons. (a) Example image of donor and acceptor cells connected within microfluidic devices. Dashed lines indicate channel boundaries. Scale bar, 30 µm. (b) Schematic of microfluidic device to investigate propagation from donor (tau^{E14}, green) to acceptor (tau^{WT}, magenta) neurons. (c) Higher magnification of white box in (a) showing intersections of donor axons and acceptor dendrites. Scale bar, 15 µm. (d) Tau^{WT} expressing acceptor neurons form aggregates when connected to tau^{E14} expressing donor neurons. (e) Neurons were transfected at DIV1 and analysed for aggregate formation. Time course of aggregate formation in axons of tau^{E14} expressing donor neurons (green circles), connected tau^{WT} expressing acceptor neurons (magenta squares), and tau^{WT} expressing neurons connected to control cells (orange triangles). N≥12 axons per experiment, 3 independent experiments per time point. Two-way ANOVA with Tukey's test, F2,60=851. Tau^{E14} (green) compared to tau^{WT} connected to tau^{E14}

(magenta) at DIV24, 26: ns p>0.999. Tau^{WT} connected to tau^{E14} (magenta) compared to tau^{WT} connected to control (orange) at DIV10: ** p=0.0028, at DIV12-26: **** p<0.0001. Error bars=SEM.

Figure 3. Differential subcompartment vulnerability to tau misfolding. (a) Acceptor somata (light grey circles) and distal axons (dark grey squares) containing tau aggregates at different time points. Each data point is the mean of one experiment, n≥8 fixed cells per time point per experiment. Two-way repeated (region) measures ANOVA, $F_{1,4}$=68.02, ns p>0.05, * p<0.05, ** p<0.01, *** p<0.001, **** p<0.0001, with *post hoc* Sidak's multiple comparison test. Error bars=SEM. (b,c) Confocal microscopy shows that (b) GFP-tau^{E14} aggregates are detected in the somata of RFP-tau^{WT} expressing acceptor neurons and overlap with RFP-tau^{WT} aggregates, while (c) RFP-tau^{WT} expressing neurons connected to GFP expressing cells do not develop aggregates. Shown are Z-projections, scale bars: 10 µm, imaged at DIV14. (d) Proximal (1,3) and distal (2,4) axonal segments of tau^{E14} and connected tau^{WT} expressing neurons were counterstained for MC1 and imaged at DIV14. Scale bar, 5 µm.

Figure 4. Neurons transmitting tau pathology remain intact. (a,b) A DIV14 tau^{E14} expressing neuron. (a) Overview of neuron stained with synapsin, nucleus stained with Hoechst 33342, and the DIC image showing an intact membrane at the cell body and along the axon. Scale bar, 30 µm. (b) The distal axons of tau^{E14} expressing neurons counterstained with synapsin. Scale bar, 10 µm. (c) Quantification of synapsin puncta per 20 µm stretch of axon. One-way ANOVA, $F_{2,6}$=0.06, p=0.82. Each data point represents the mean of one experiment, with n=45 axons total (untransfected, tau^{E14}) and 35 axons total (tau^{WT}).

Figure 5. Tau^{E14} expressing neurons show selective axonal dysfunctions at DIV14. Imaging of lysosomes at the distal axon reveals (a,b) a reduction in the number of lysosomes (indicated by white arrows) in tau^{E14} expressing distal axons compared to tau^{WT} expressing cells. N=8 cells per experiment, each point is the mean of one experiment. T-test, df=4, t=7.44, p=0.0017. (c-e) Analysis of lysosome dynamics in tau^{E14} and tau^{WT} expressing axons. (c,d) Representative kymographs of tau^{WT} and tau^{E14} expressing axons. (e) Transport analysis of lysosomes. Each data point is the mean of one experiment, n≥8 cells per experiment. Error bars=SEM. One-tailed t-test, df=4, t=6.14, p=0.0018.

Figure 6. Tau^{E14} neurons are electrically competent. (a,b) Basal calcium activity of a DIV14 (a) tau^{WT} (b) and tau^{E14} expressing neuron, which is silenced on application of 1 μM TTX. Addition of 100 mM KCl confirms viability at the end of acquisition. (c-f) Electrophysiology on DIV14 neurons. (c) Sample traces of current injection into patch clamped neurons. (d) Rheobase of tau^{WT} and tau^{E14} expressing neurons show a similar minimal current is required for action potential initiation. T-test, df=4, t=0.24, p=0.82. (e) Input resistance of tau^{WT} and tau^{E14} expressing neurons shows no significant difference. T-test, df=4, t=0.53, p=0.62. (f) Resting membrane potentials recorded for tau^{WT} and tau^{E14} expressing neurons. T-test, df=4, t=0.20, p=0.85. For (d-f), N≥3 cells per experiment, each point = median of 1 experiment.

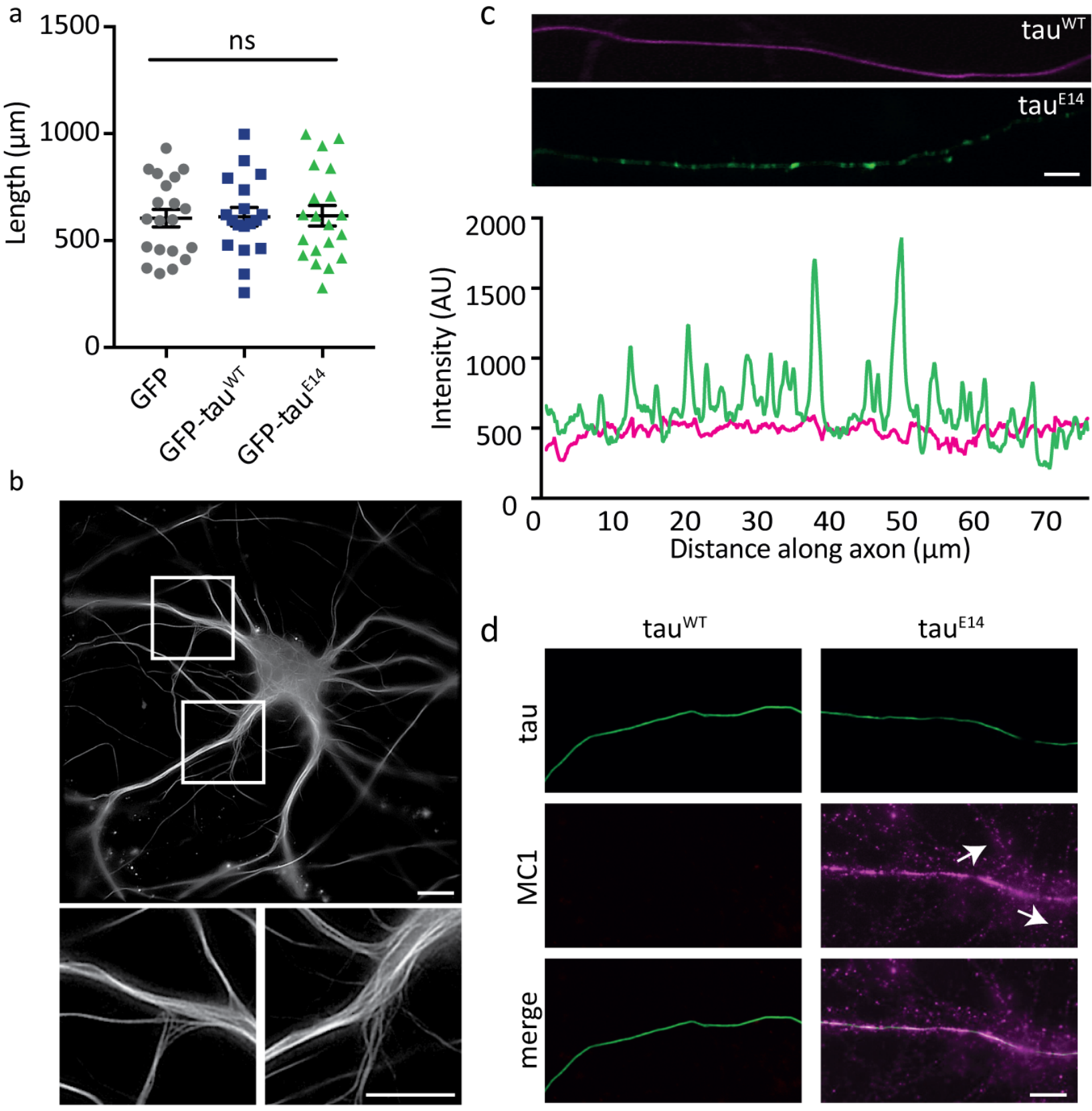
a
1500
1000
500
0
Length (µm)
ns
GFP
GFP-tau^WT
GFP-tau^E14
b
c
tau^WT
tau^E14
2000
1500
1000
500
0
Intensity (AU)
0
10
20
30
40
50
60
70
Distance along axon (µm)
d
tau^WT
tau^E14
tau
MC1
merge

Figure 1

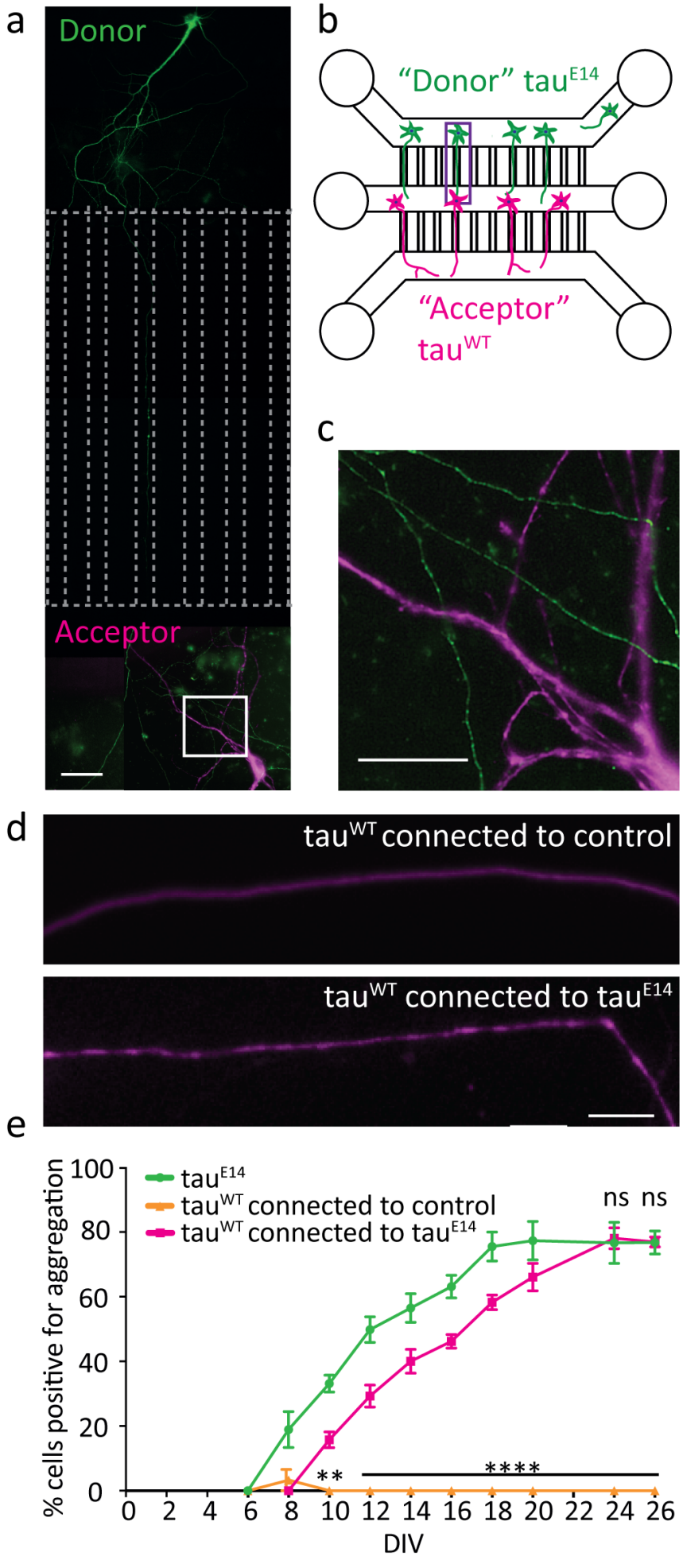
a
Donor
Acceptor
b
"Donor" tau^{E14}
"Acceptor"
tau^{WT}
c
d
tau^{WT} connected to control
tau^{WT} connected to tau^{E14}
e
% cells positive for aggregation
100
80
60
40
20
0
tau^{E14}
tau^{WT} connected to control
tau^{WT} connected to tau^{E14}
ns ns
**
****
0 2 4 6 8 10 12 14 16 18 20 22 24 26
DIV

Figure 2

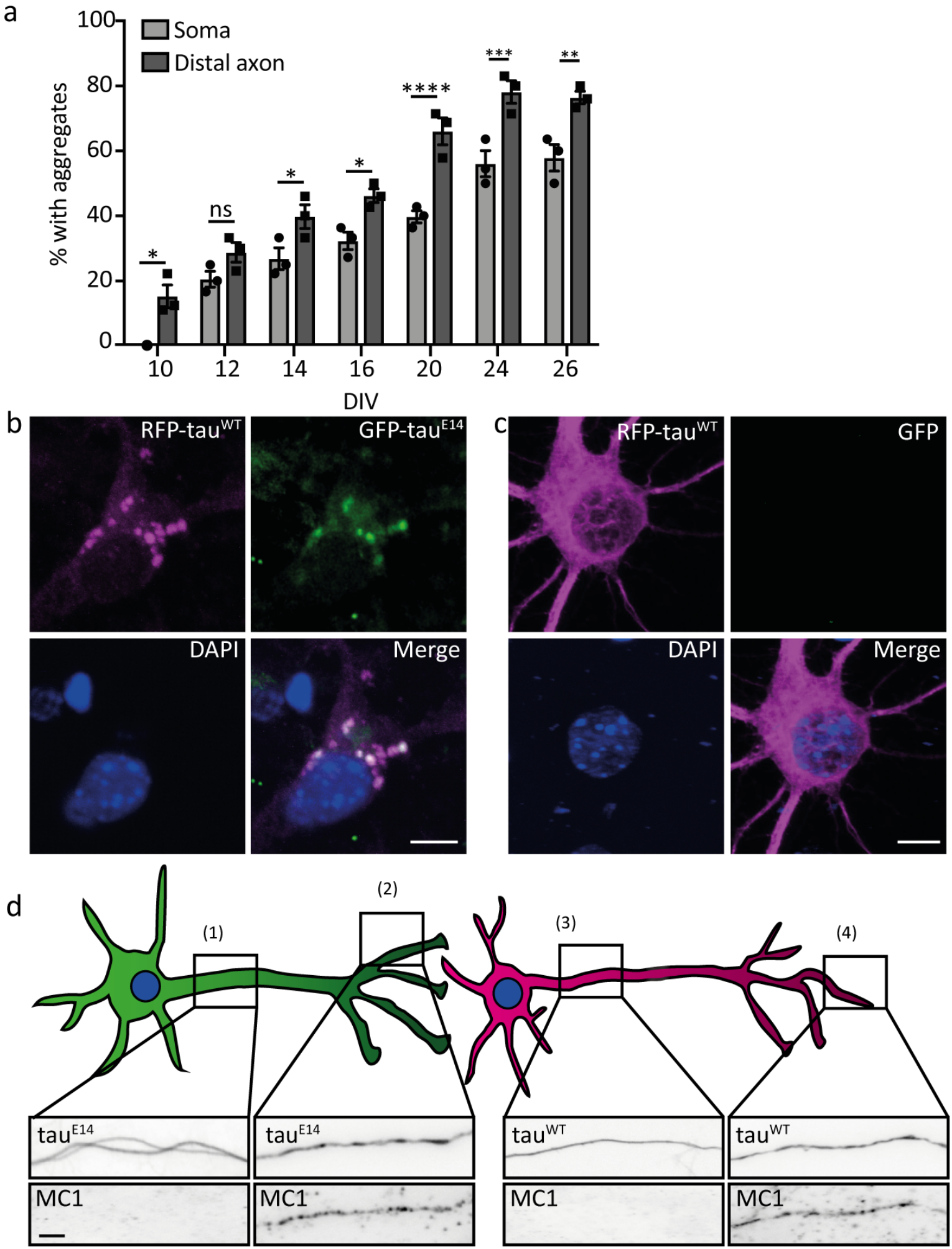
a
100
80
60
40
20
0
% with aggregates
Soma
Distal axon
*
ns
*
*
****
***
**
10
12
14
16
20
24
26
DIV
b
RFP-tau^WT
GFP-tau^E14
DAPI
Merge
c
RFP-tau^WT
GFP
DAPI
Merge
d
(1)
(2)
(3)
(4)
tau^E14
tau^E14
tau^WT
tau^WT
MC1
MC1
MC1
MC1

Figure 3

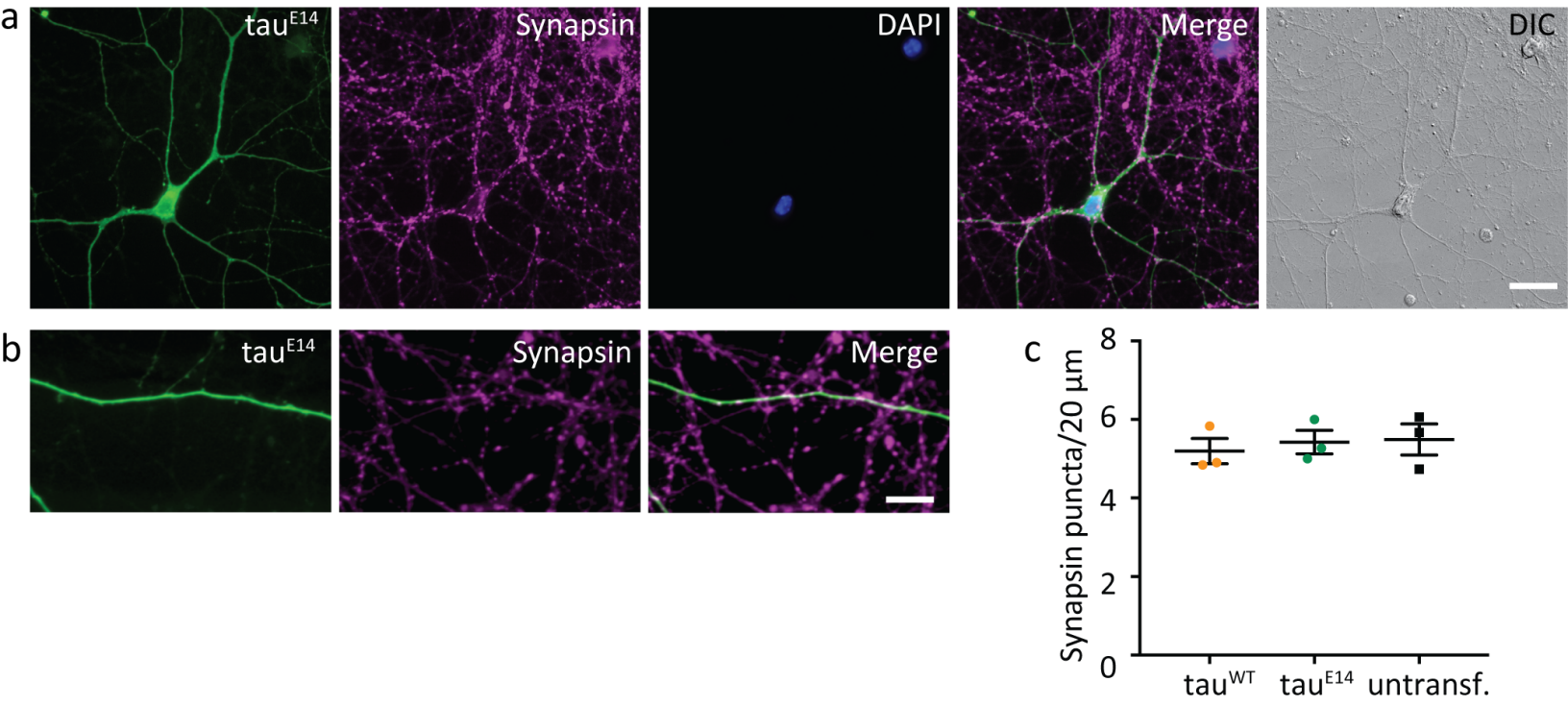
a
tau^E14
Synapsin
DAPI
Merge
DIC
b
tau^E14
Synapsin
Merge
c
Synapsin puncta/20 µm
0
2
4
6
8
tau^WT
tau^E14
untransf.

Figure 4

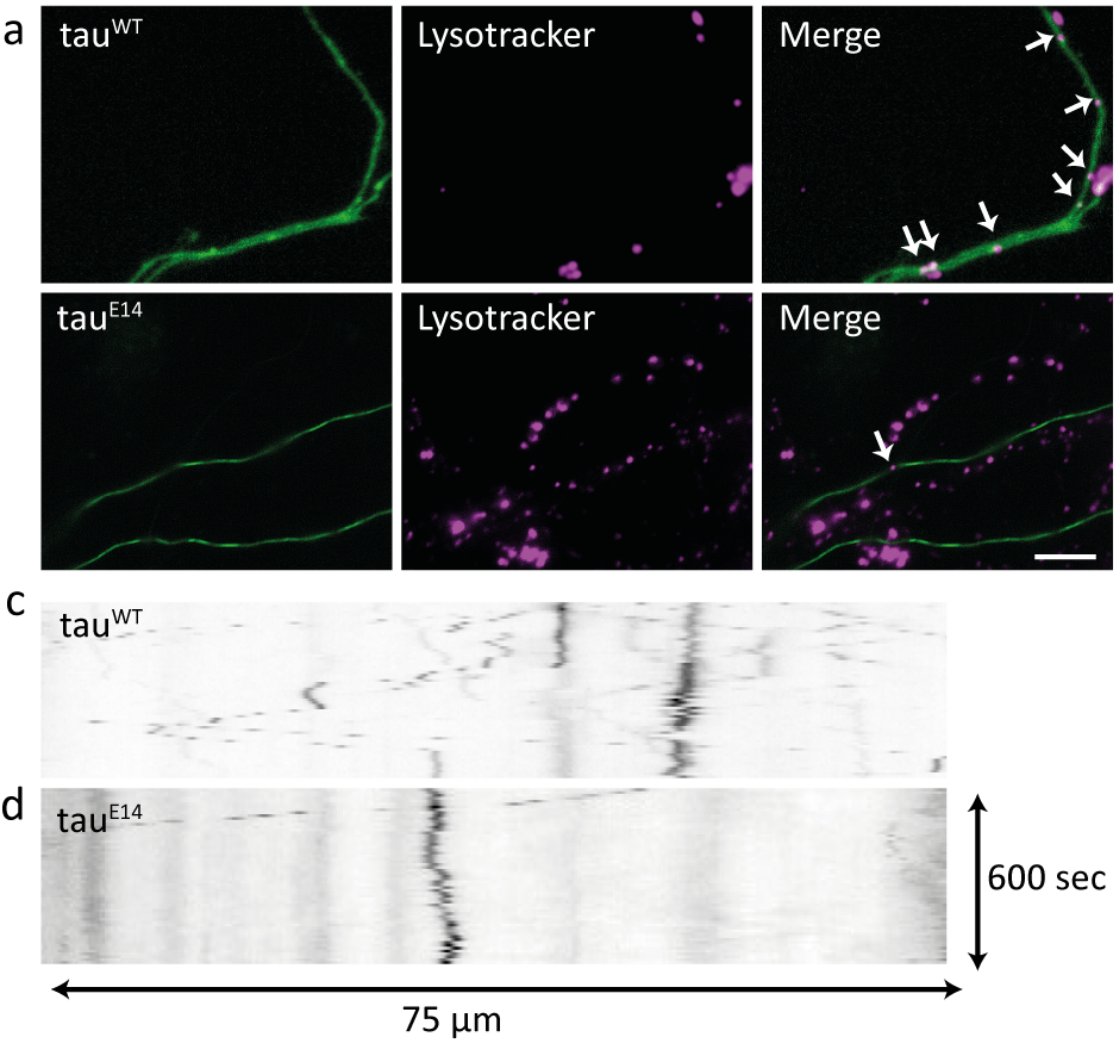
a
tau^WT
Lysotracker
Merge
tau^E14
Lysotracker
Merge
b
**
Number/ 75µm
12
10
8
6
4
2
0
tau^WT
tau^E14
c
tau^WT
d
tau^E14
600 sec
75 µm
e
100
80
60
40
20
0
% moving
**
tau^WT
tau^E14

Figure 5

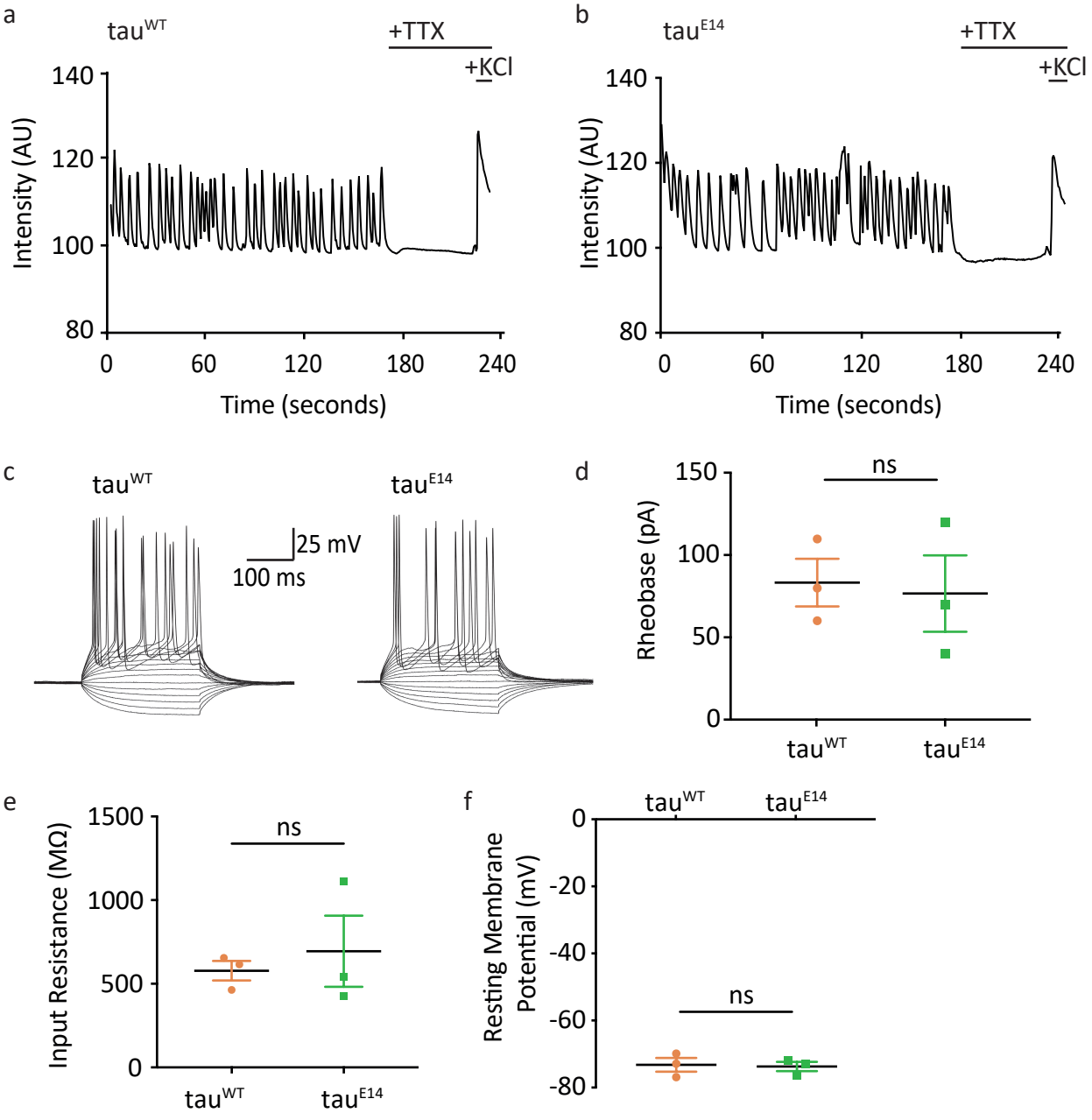
a
tauWT
+TTX
+KCl
Intensity (AU)
140
120
100
80
0
60
120
180
240
Time (seconds)
b
tauE14
+TTX
+KCl
Intensity (AU)
140
120
100
80
0
60
120
180
240
Time (seconds)
c
tauWT
tauE14
25 mV
100 ms
d
Rheobase (pA)
150
100
50
0
ns
tauWT
tauE14
e
Input Resistance (MΩ)
1500
1000
500
0
ns
tauWT
tauE14
f
tauWT
tauE14
Resting Membrane Potential (mV)
0
-20
-40
-60
-80
ns

Figure 6